

PAPER

Transport and topological properties of ThOCh(Ch: S, Se and Te) in bulk and monolayer: a first principles study

To cite this article: Vineet Kumar Sharma *et al* 2019 *J. Phys.: Condens. Matter* **31** 435504

View the [article online](#) for updates and enhancements.



IOP | ebooks™

Bringing you innovative digital publishing with leading voices to create your essential collection of books in STEM research.

Start exploring the collection - download the first chapter of every title for free.

Transport and topological properties of ThOCh(Ch: S, Se and Te) in bulk and monolayer: a first principles study

Vineet Kumar Sharma¹, P C Sreeparvathy¹, P Anees² and V Kanchana¹ 

¹ Department of Physics, Indian Institute of Technology Hyderabad, Kandi—502285, Sangareddy, Telangana, India

² Materials Physics Division, Indira Gandhi Centre for Atomic Research, Kalpakkam 603702, India

E-mail: kanchana@iith.ac.in

Received 8 April 2019, revised 19 June 2019

Accepted for publication 28 June 2019

Published 30 July 2019



Abstract

The present study unveils the topological insulating nature of Th-based oxy-chalcogenides and their transport properties which are less explored. A systematic analysis of electronic, topological, mechanical, dynamical and thermoelectric properties of ThOCh (Ch: S, Se and Te) in bulk and monolayer is presented. The effect of spin–orbit coupling is found to be appreciable in ThOTe compared to ThOS and ThOSe, causing a strong topological nature in bulk ThOTe. The detailed analysis of electronic structure, Z_2 topological invariant and conducting surface states support the strong topological nature in bulk ThOTe. From thermoelectric studies, ThOS and ThOSe are found to be good thermoelectric candidates with heavy carrier doping (around 10^{20} cm^{-3}). To explore further, we have applied hydrostatic strain on bulk ThOCh and found that all the compounds are dynamically stable and show topological metallic behavior. The appearance of highly linearized Dirac points in the same energy range at different high symmetry points in the BZ indicate the presence of nodal line in ThOS and ThOSe without spin–orbit coupling and with the inclusion of spin–orbit coupling, the nodal line is found to be disappear. This variation in bands with and without spin–orbit coupling might indicate the topological nature in monolayer ThOCh. The thermoelectric calculations for monolayer shows an enhancement in electrical conductivity scaled by relaxation time by an order of ten compared to bulk and the carrier independent thermoelectric properties in monolayer might fetch good thermoelectric device applications. Overall, the present study explores yet another series of potential candidates for topological and thermoelectric properties in both bulk and layer forms.

Keywords: electronic structure, topological materials, thermoelectric properties

 Supplementary material for this article is available [online](#)

(Some figures may appear in colour only in the online journal)

1. Introduction

The search for thermoelectric materials has grown in recent years due to concerns about global warming and gathered the attention of researchers because of their technological applications such as waste heat recovery and thermoelectric power generation. Although, numerous noble materials are found in

this area of research, the performance of these materials is still a big challenge. The key point is to enhance the thermoelectric performance of such materials which is characterized by a dimensionless quantity called figure of merit. The figure of merit, $ZT = \sigma S^2 T / \kappa$, where σ , S , T and κ are electrical conductivity, the thermopower, the absolute temperature and thermal conductivity respectively. Here, $\kappa = \kappa_e + \kappa_l$, where

the former one is electronic thermal conductivity and latter one is lattice thermal conductivity. The basic requirements for good thermoelectric material are large thermopower, high electrical conductivity and low thermal conductivity, and achieving this condition is a challenging task due to the inter-related parameters. One of the recent studies on ThTaN₃, has reported a topological crystalline insulator with high thermopower [1]. Well known thermoelectric materials like Bi₂Se₃ and Bi₂Te₃ were reported as topological insulators [2–4]. The co-existence of multiple applications are fruitful, and gather enormous attraction. The recent discovery of topological insulators was a great breakthrough in materials science world [5–7]. Topological insulator is a kind of material which has insulating gap in bulk and possess conducting surface states [8, 9]. The amalgamation of complex bulk band structure and exotic surface states result in enhancing several properties such as thermoelectric energy conversion, superconductivity, extreme magneto-resistance etc [10–12].

To explore novel topological materials, several methods have been proposed within the frame work of first principles calculations. Topological materials are in general classified as topological insulators, semi-metals, crystalline insulators etc [13]. Another class of topological material called topological metal has not been explored adequately so far. Lucas Muechler *et al*, studied the importance of spin–orbit coupling in non-symmorphic topological metals with band inversion in bulk as well as monolayer and bilayer [14]. Recently, chalcogen based layered compounds have drawn attention because of the transition in their electronic properties from bulk to monolayer. Another interesting fact about chalcogenides is that their electronic properties can be tuned not only by cleaving but also by strain engineering [15, 16]. In general, chalcogenides possess high thermopower and low thermal conductivity [17, 18] which are ideal features of a thermoelectric material. Few other transition metal dichalcogenides such as TiS₂ and TiTe₂ studied using *ab initio* calculations reported the topological phase in certain doping range for TiS_{2–x}Te_x in both bulk and monolayer forms [19]. We have chosen thorium based oxy-chalcogenides for the present study which are less explored.

Despite the fact that thorium is radioactive element, lots of research has been carried out on thorium based mono-chalcogenides and mono-pnictides which crystallize in cubic structure [20]. Since thorium belongs to family of elements having heavy nuclei, its compounds possess high density and high melting point. These properties make them suitable for applications in nuclear reactors. Binary compounds of thorium has been studied at large scale due to their peculiar chemical and physical properties [21–24]. Yong Xu *et al*, reported that the thermoelectric performance of materials can be enhanced by tuning the size parameter in topological insulators [25]. Several studies have already been performed, which resulted in many topological materials with PbFCl type, structure [26, 27]. Lucasz *et al* [28] has investigated the electronic and optical properties of thorium oxychalcogenides ThOCh(Ch: S, Se, Te). Previously, many chalcogenide based compounds were studied and found to have both thermoelectric and topological nature [29–31]. These studies gave the insight about their combination of thermoelectric and topological properties

in same materials and can be utilized for large scale applications in devices, which serve as the motivation for present work. The investigated compounds were earlier explored for doping effects, thermal properties and optical properties [28], but thermoelectric and topological studies have not been discussed so far. Here, we intend to investigate the topological and thermoelectric properties of ThOCh in both bulk and monolayer forms, and also aim to analyse the effect of strain on the investigated compounds.

2. Methods

Geometry optimization for all the investigated compounds has been carried out using pseudopotential method as implemented in VASP package [32, 33]. Phonon calculations were performed using the combination of phonopy code [34] and density functional perturbation theory(DFPT) [35] as implemented in VASP. The electronic structure properties are calculated using self consistent FP-LAPW method as implemented in WIEN2k [36] package. The PBE-GGA [37](Perdew–Burke–Ernzerhof parametrization of the generalized gradient approximation) was used for the exchange correlation functional. The convergence criteria for energy was set as 10^{–6} Ry. The electronic structure calculations has been carried out with a k-mesh of 21 × 21 × 12 according to Monkhorst–Pack scheme [38]. In-order to analyze the topological nature, we have computed the surface band structure, using maximally localized Wannier functions [MLWFs] [39]. Firstly, the tight binding Hamiltonian is constructed using MLWFs in conjunction with VASP code. Further, the tight binding parameters are fed to WannierTools [40] package, which employs an iterative Green’s function [41] technique to obtain the surface state properties. Z₂ topological invariants were calculated from the converged VASP outputs. A higher k-mesh of 44 × 44 × 25 is used for transport calculations. We have employed the semi-classical Boltzmann transport theory on our converged calculations as implemented in BoltzTraP code [42] to compute thermoelectric properties. Thermoelectric properties such as thermopower, electrical conductivity scaled by relaxation time and power factor scaled by relaxation time are being calculated within the constant scattering time approximation (CSTA) and rigid band approximation (RBA) [43–45]. Further, we have calculated the lattice thermal conductivity with the combination of phono3py [46] and VASP. Supercell approach has been used to calculate the second and third force constants.

3. Results and discussions

3.1. Structural and electronic properties at ambient condition

The investigated compounds are found to have a layered PbFCl type structure and crystallize in tetragonal system with space group *P4/nmm*. The schematic of the crystal structure is given in figure 1(a). The optimized lattice parameters are given in table 1 for all the compounds along with experimental and other theoretical values and are in good agreement with experiment. Since ‘Th’ is a heavy element, the effect of spin–orbit

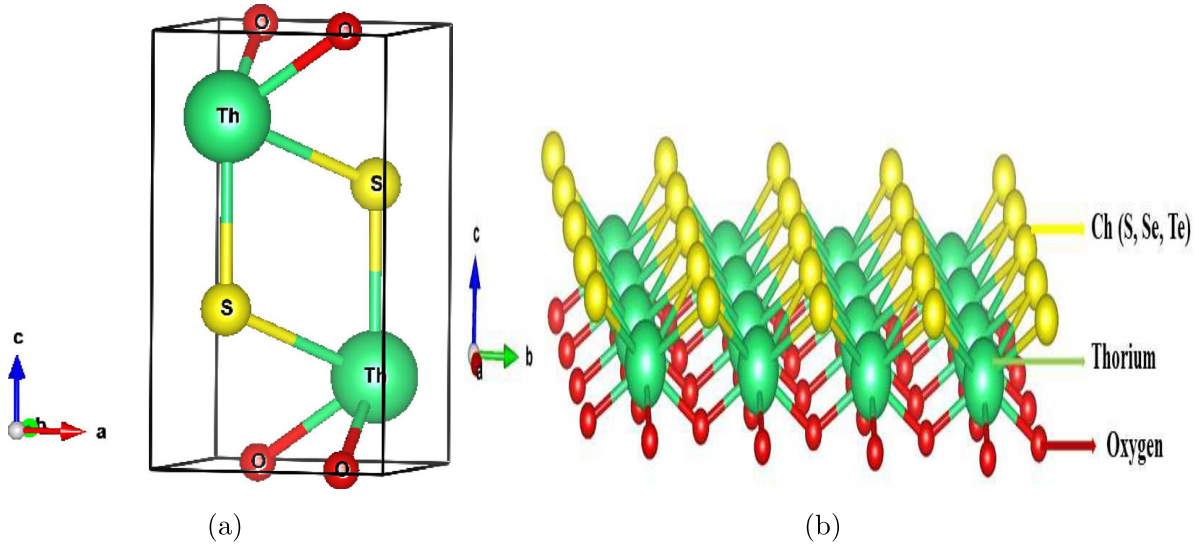


Figure 1. Crystal structure for ThOCh (a) Bulk structure (b) Monolayer structure.

Table 1. Optimized lattice parameters ‘a’ and ‘c’ along with experimental parameters for ThOS, ThOSe and ThOTe.

Parameters	ThOS		ThOSe		ThOTe	
	Experiment	Present work	Experiment	Present work	Experiment	Present work
a (Å)	3.95 ^a	3.96	4.01 ^a	4.03	4.11 ^a	4.13
c (Å)	6.74 ^a	6.75	7.01 ^a	7.05	7.52 ^a	7.59

^a [28].

coupling is significant in these compounds, and we have included the same in our calculations. The band structures of ThOCh (Ch: S, Se, Te) with and without inclusion of spin-orbit coupling are presented in figures 2(a)–(c). The impact of spin-orbit coupling is found to increase from S to Te, and the band profile is almost similar in the case of ThOS and ThOSe, where the degeneracy of bands are lifted up with spin orbit coupling. Here, ThOTe is found to stand out separately, where the band profile has been altered with the inclusion of spin-orbit coupling. From the calculated electronic structure properties, it is found that these compounds are semiconductors as reported earlier [28]. ThOS and ThOSe are found to be direct band gap semiconductor with band gap values around 1.1 eV and 0.7 eV respectively, but in ThOTe the band profile is altered by the effect of spin orbit coupling, and the indirect band gap is around 0.17 eV. Further analysis has been performed with the inclusion of spin-orbit coupling. We could see that the valence band is more populated than conduction band near Fermi level at Γ point enabling more hole carriers than the electrons (figure 2). In addition, the valence band is dominated by p-orbitals of both O and Ch(S, Se and Te) and conduction band is dominated by Th ‘f’ and ‘d’ states, which is evident from density of states as presented in figure 3. The variation of density of states near the Fermi level clearly indicates that, hole doped thermopower will be more pronounced for ThOS and ThOSe, which will be examined in the later section. Since the investigated compounds crystallize in tetragonal structure, we have analysed the possibility of anisotropic nature through band structure and effective mass calculations (table 2). The band dispersion along different crystallographic

directions is found to be different and the same is reflected in effective mass values. The bands are less dispersed along Γ –Z compared to Γ –X, which might induce anisotropy in the transport properties. The combination of narrow band gap and highly influential spin-orbit coupling effect motivate us to check the possibility of topological non-trivial states in these compounds. For this purpose, we have calculated the projected band structure, which is presented in figures 2(d)–(f). From figure 2(d), it is quite evident that ‘d’ states are dominant in the conduction band and ‘p’ states are found to be pronounced in the valence band for ThOS. The projected band structure of ThOTe with and without spin-orbit coupling is given in figures 2(f) and (g) respectively. We could observe a band character flipping driven by spin-orbit coupling around Γ point, which indicate the band inversion in ThOTe. We have confirmed the presence of time reversal symmetry in all the investigated compounds by performing spin-polarized calculations. Since all the investigated compound preserve both time reversal symmetry and inversion symmetry, it is possible to connect the Z_2 topological invariant with the parity of Bloch wave functions. For this purpose, we have adapted the method proposed by Fu and Kane [47]. We have calculated the parity at eight TRIM points for all occupied bands in the Brillouin zone and analysed the Z_2 invariant through parity. The calculated Z_2 invariant are represented in table 3. From the table it is evident that, ThOSe is a weak topological insulator and ThOTe is a strong topological insulator. From the projected band analysis, we could notice a band character flipping for ThOTe, and for further evidence, we have calculated surface states for ThOTe using wannier90. Well converged

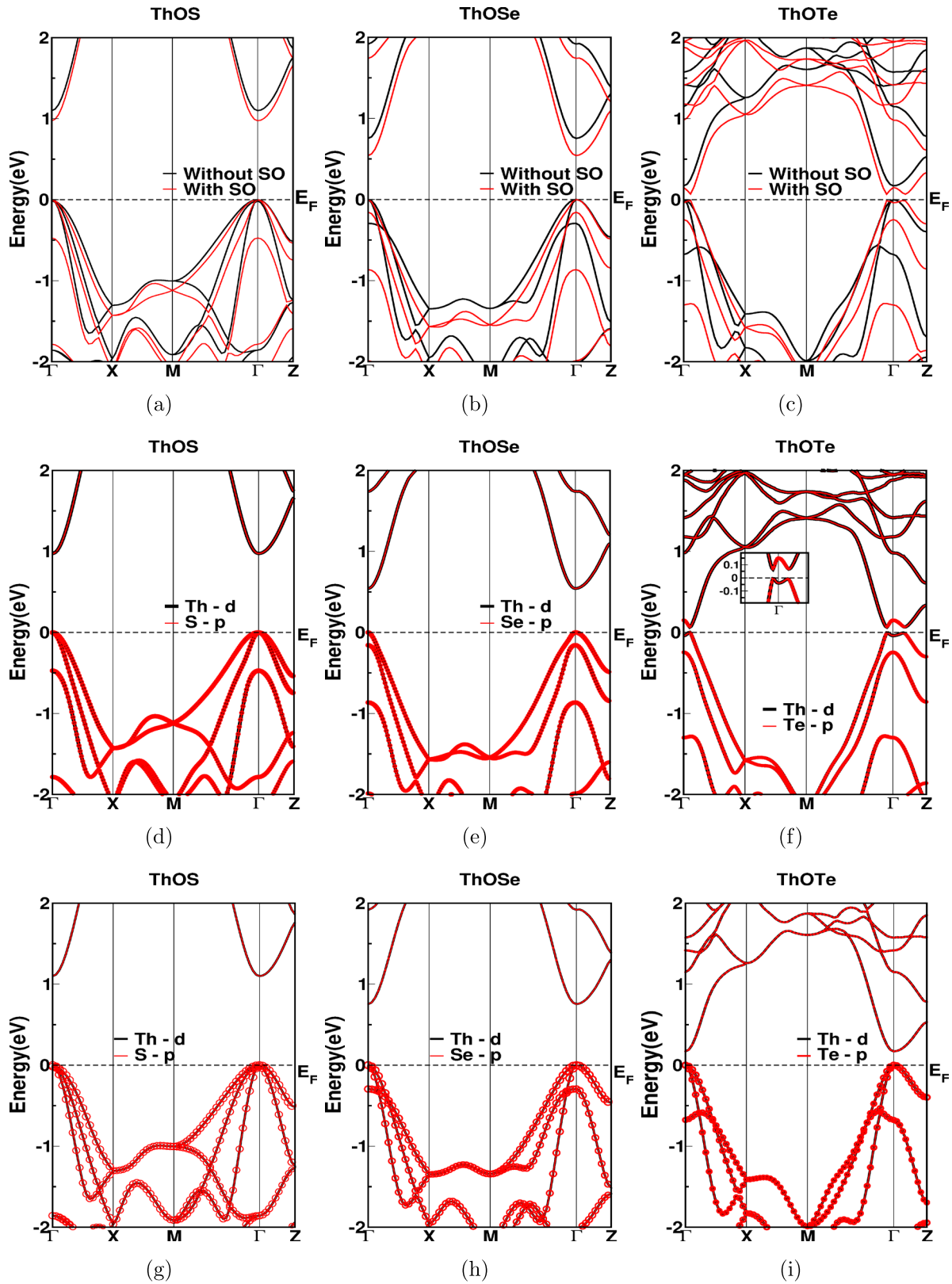


Figure 2. Band structure calculated in bulk with and without spin–orbit coupling for ThOS (a), ThOSe (b) and ThOTe (c), and Projected band structure calculated with spin–orbit coupling for ThOS (d), ThOSe (e) and ThOTe (f), and without spin–orbit coupling for ThOS (g), for ThOSe (h), for ThOTe (i).

output from VASP has been taken into wannier90 and further Wanniertools are used to generate the surface band structure. Here, we have calculated surface states along (001) plane,

and the surface bands are highly dispersive. The highly linearized Dirac like points as well as the band flipping character similar to that of bulk can be seen around Γ high symmetry

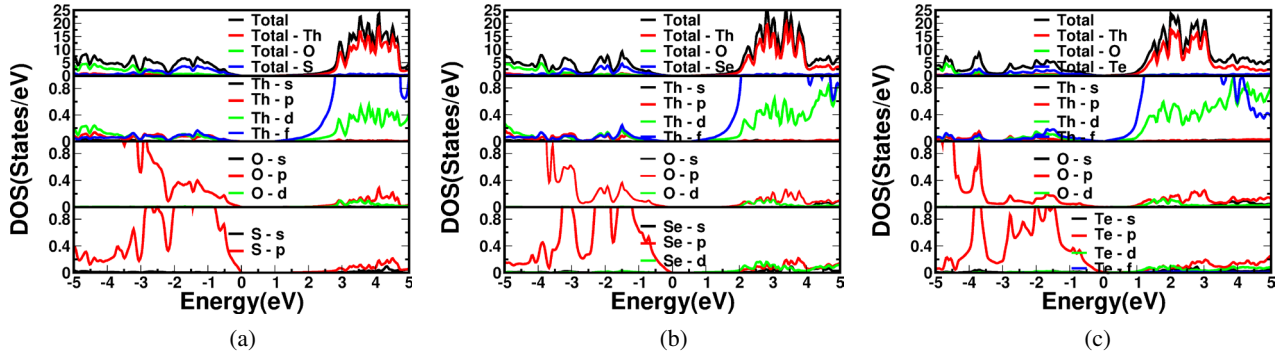


Figure 3. Density of states calculated in bulk for ThOS (a), ThOSe (b) and ThOTe (c).

Table 2. Effective mass in the unit of electron mass(m_e) calculated along Γ -X and Γ -Z for compounds ThOS, ThOSe and ThOTe.

Effective mass	ThOS		ThOSe		ThOTe	
Path	$M_h(m_e)$	$M_e(m_e)$	$M_h(m_e)$	$M_e(m_e)$	$M_h(m_e)$	$M_e(m_e)$
Γ -X	0.69	0.47	0.58	0.44	0.08	0.07
Γ -Z	1.05	0.92	0.81	1.64	3.90	1.24

Table 3. Wave function parities calculated along with Z_2 for the compounds ThOS, ThOSe and ThOTe.

Compound	Γ	X	X	Z	$\nu_0; \nu_1 \nu_2$ ν_3
ThOS	-1	1	1	-1	(0;0 0 0)
ThOSe	-1	-1	-1	1	(0;1 0 0)
ThOTe	1	1	1	1	(1;1 0 0)

Table 4. Elastic constants and mechanical properties calculated for the compounds ThOS, ThOSe and ThOTe. Here, G is the shear modulus which is the average of shear moduli G_V and G_R calculated using Voigt and Ruess approximation respectively and E is the Young modulus.

Elastic Properties	ThOS	ThOSe	ThOTe
C_{11} (GPa)	232.479	232.393	232.391
C_{12} (GPa)	90.034	89.931	89.934
C_{13} (GPa)	100.207	100.604	100.479
C_{33} (GPa)	186.153	185.323	185.212
C_{44} (GPa)	79.466	79.411	79.605
C_{66} (GPa)	63.098	63.100	63.125
B (GPa)	136.85	136.39	136.60
G_V (GPa)	68.45	68.33	68.45
G_R (GPa)	66.00	65.93	65.91
G (GPa)	67.18	67.13	67.11
G/B	0.4918	0.4924	0.4923
E(GPa)	173.19	173.01	172.98
σ	0.2897	0.2885	0.2888
A_U	1.16	1.11	1.11
θ_D (K)	314.45	294.1	279.88

point which confirm the exotic surface states and it is evident from figure 4. The combination of band inversion, non zero Z_2 topological invariant and exotic surface states confirm the strong topological nature of ThOTe.

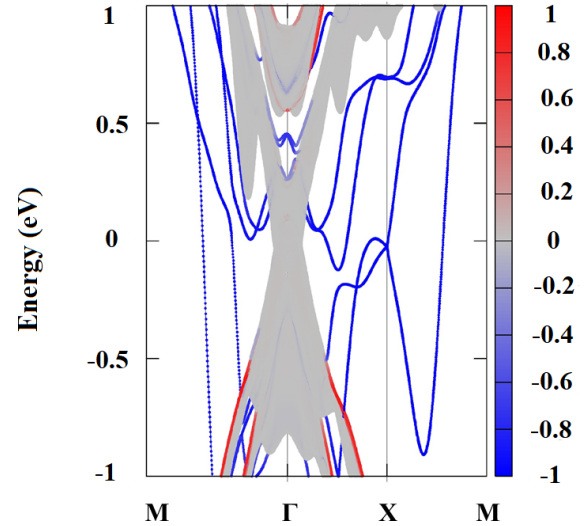


Figure 4. Surface bands calculated for ThOTe in bulk.

3.2. Mechanical and dynamical properties

To understand the mechanical and dynamical properties of the investigated compounds, we have calculated the elastic constants and phonon dispersion. Calculated elastic constants are tabulated in table 4 which satisfy Born's stability criteria [48]. From the calculated single crystal elastic constants, we can calculate macroscopic elastic moduli for all systems and the polycrystalline elastic properties can be calculated from first principles with Voigt–Reuss–Hill approximation [49]. Here, G is the shear modulus, the average of shear moduli G_V and G_R calculated using Voigt and Ruess approximation respectively. G/B ratio is less than 0.5 for all the compounds, which indicates the ductility of the investigated compounds. Calculated Debye temperature of ThOS, ThOSe and ThOTe are 314.45 K, 294.1 K and 279.99 K respectively. These values are comparable with well established thermoelectric materials with low thermal conductivity [50, 51] which implies that the present

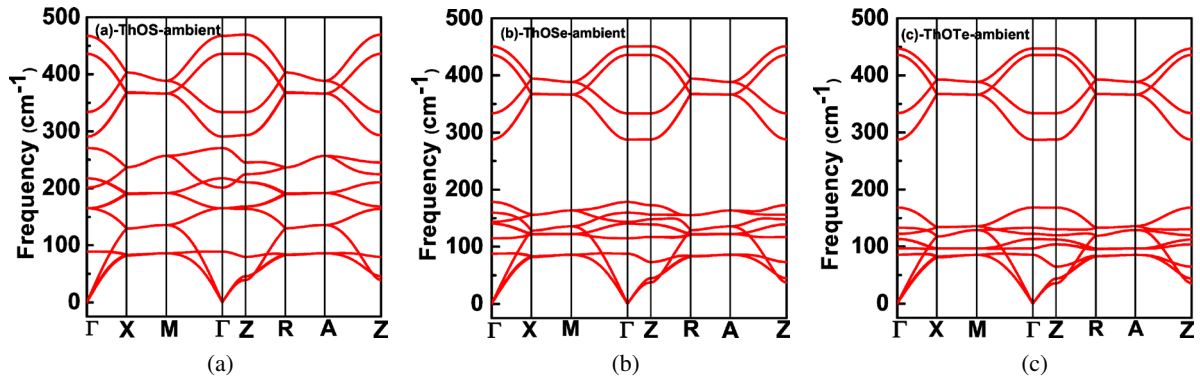


Figure 5. Calculated phonon dispersion for ThOS (a), ThOSe (b) and ThOTe (c) in bulk.

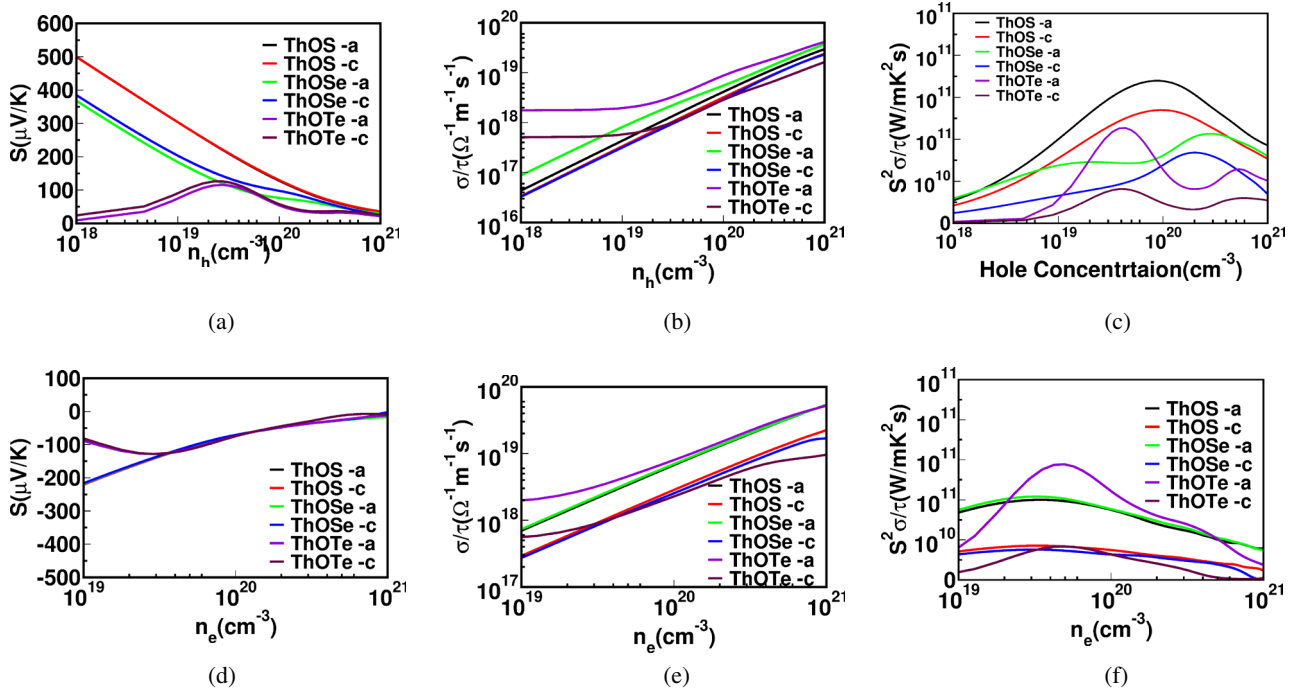


Figure 6. Thermoelectric properties for bulk structure calculated as a function of carrier concentration, Thermopower (a) and (d), electrical conductivity scaled by relaxation time (b) and (e), power factor scaled by relaxation time (c) and (f).

compounds might be expected to possess low thermal conductivity. Further, we have analysed the dynamical stability of these compounds by calculating the phonon dispersion along the high symmetry directions, and is represented in figure 5. The obtained positive frequencies of all the compounds confirm the dynamical stability. The maximum range of phonon frequency is found to decrease from ThOS to ThOTe, where in ThOS the maximum frequency is around 470 cm^{-1} , and the same for ThOTe is around 448 cm^{-1} , which might be due the presence of heavy element in ThOTe. Though all the investigated compounds crystallize in same structure, few differences are observed in the phonon dispersion plot. In the case of ThOS, a small phonon gap of 20 cm^{-1} is observed at higher frequencies, whereas in the case of other two compounds the presence of large phonon gap around 100 cm^{-1} is observed. The large mass difference between Te and O and Se and O might be the reason for this huge phonon gap. Further, in ThOSe and ThOTe, low frequency optical modes are found to be highly interactive with acoustic modes, which might increase the

phonon scattering and hence decrease the lattice thermal conductivity, and the presence of highly flat phonon modes may also support a similar trend of low thermal conductivity. The optical and acoustic phonon modes interaction is observed in ThOSe and ThOTe around 100 cm^{-1} , and for ThOS it is observed around 170 cm^{-1} .

3.3. Thermoelectric properties

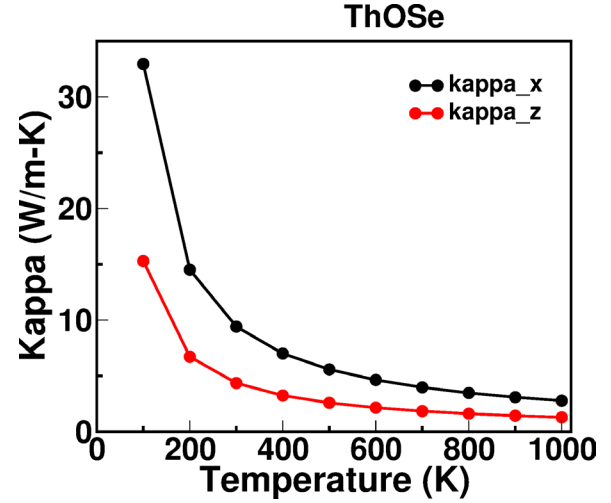
We have calculated thermoelectric properties for all the investigated compounds as a function of carrier concentration. Since these systems are tetragonal, we have calculated thermoelectric properties along 'a' and 'c' axis where 'a' corresponds to 'x' axis and 'c' corresponds to 'z' axis. The magnitude of thermopower for hole doping is observed in the range of $100\text{--}500\text{ }\mu\text{V K}^{-1}$, and for electron doping, the maximum value is up to nearly $250\text{ }\mu\text{V K}^{-1}$ for temperature around 300 K at ambient as shown in figures 6(a) and (d). High value of thermopower for holes might be due to that flat band and heavy

Table 5. Minimal thermal conductivity calculated for the compounds ThOS, ThOSe and ThOTe.

Compound	K_{\min} (W mK ⁻¹)
ThOS	0.88
ThOSe	1.11
ThOTe	0.73

mass residing below Fermi level. This is confirmed from the electronic structure properties and effective mass calculated along different crystallographic directions (table 2). We have calculated thermopower for temperatures ranging from 300 K to 700 K. At very high temperature more than 500 K, slight bipolar conduction is being observed at low carrier concentrations for ThOS. The bipolar conductivity is related to band gap. If the band gap is less, the carriers can easily cross Fermi level as temperature increases and in such condition, both kind of carriers contribute to thermopower, which suppress the net thermopower. The variation of thermopower as a function of carrier concentration for ThOS is given in figures 6(a) and (d) and from the figure, it is evident that the magnitude of thermopower is decreasing with carrier concentration, which is the basic trend in semiconductors. Similar trend is observed for ThOSe, and the thermopower is around 500 $\mu\text{V K}^{-1}$ for holes and 200 $\mu\text{V K}^{-1}$ for electrons at 300 K. Beyond 500 K, this compound has shown increased bipolar conduction than ThOS, but in the concentration range around 10^{19} – 10^{21} cm^{-3} . For ThOTe, we have observed the presence of bipolar conduction at low temperature itself (figure 6). The calculated thermopower is found to be isotropic. Next, we have analysed the electrical conductivity scaled by relaxation time, which is given in figures 6(b) and (e). This shows linear behavior as a function of carrier concentration and a small anisotropic behavior is observed in calculated electrical conductivity scaled by relaxation time, as expected from the highly dispersed electronic band structure. Further, we have analysed the power-factor as a function of carrier concentration and presented the same in figures 6(c) and (f). For both hole and electron doping, the maximum power-factor is obtained around 5×10^{10} W mK⁻²s for all the compounds at 300 K for carrier concentration ranging between 10^{19} – 10^{20} cm^{-3} . ThOSe has almost same power factor scaled by relaxation time as that of ThOS. Since we have observed bipolar conduction in case of ThOTe, it leads to lesser power factor scaled by relaxation time. To understand the high temperature behavior, we have presented the thermoelectric properties at 700 K in supplementary figure 1 (stacks.iop.org/JPhysCM/31/435504/mmedia). From the figure it is evident that at higher carrier concentrations, both ThOS and ThOTe secured appreciable thermopower at higher temperature, where in ThOTe we could see bipolar conduction in all the studied range of concentration. We have attempted to calculate the minimal thermal conductivity for the investigated compounds using analytical relation given by Clarke [52, 53]. The minimal thermal conductivity according to Clarke's model is given by,

$$k_{\min} = 0.87 \times k_B M_a^{-2/3} E^{1/2} \rho^{1/6}.$$

**Figure 7.** Thermal conductivity of ThOSe calculated as a function of temperature.

Here, ' M_a ' = $[M/m \cdot N_A]$ is the average mass per atom, ' E ' is the Young's modulus, ' ρ ' is the density, ' M ' is the molar mass, ' m ' is the total number of atoms per formula, ' k_B ' is Boltzmann constant, ' N_A ' is Avogadro's number, ' n ' is number of atoms per unit volume. The minimal thermal conductivity of the investigated compounds are 0.88, 1.11, 0.73 W mK⁻¹ respectively (table 5), and these values are being cross-checked with the values available for established thermoelectric systems [54, 55], and are found to be in good accord with them.

Force constant method is one of the efficient method to predict the lattice thermal conductivity. Next, we have calculated thermal conductivity of ThOSe as a function of temperature using third order force constants, which includes anharmonic terms also in the Hamiltonian. Calculated temperature dependent thermal conductivity is presented in figure 7. From the plot, thermal conductivity is found to decrease with temperature. We have observed anisotropic nature in thermal conductivity at low temperature which is reducing as the temperature increases. Obtained anisotropy in lattice thermal conductivity can be connected to the structural anisotropy. The calculated thermal conductivities are around 9 W mK⁻¹ and 4 W mK⁻¹ along ' a ' and ' c ' axis respectively at 300 K. The calculated thermal conductivities are comparable with earlier reported work on half-Heusler alloys [56, 57].

4. Strain effects

We have employed hydrostatic compressive strain on these compounds causing the reduction in band gap. As a result, ThOS and ThOSe turned into metal at 10% strain and ThOTe at 5% strain. The phonon dispersion calculations at these strained states confirm the dynamical stability, and are given in figures 8(a)–(c). From the phonon spectrum, we can visualize softening of phonons along Γ -Z, but this softening is lesser than that found at ambient.

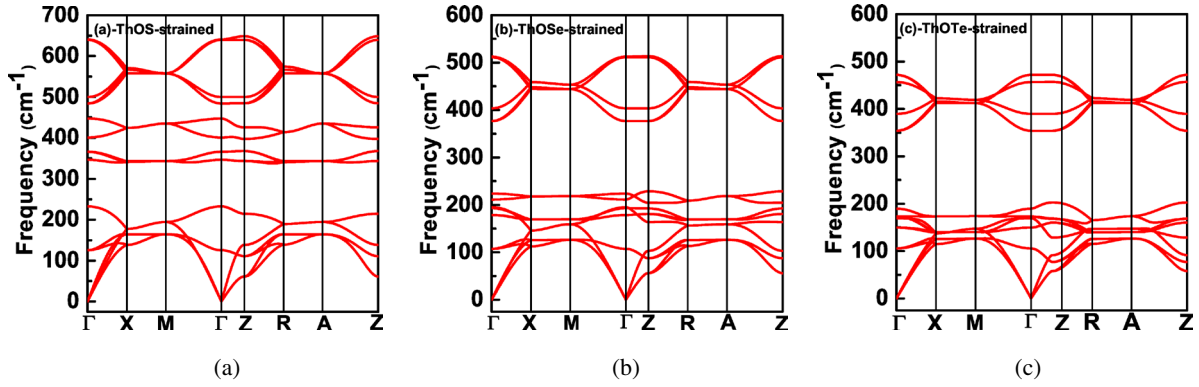


Figure 8. Calculated phonon dispersion with compressive strain for ThOS (a), ThOSe (b) and ThOTe (c) in bulk.

Table 6. Wave function parities calculated along with Z_2 for the compounds ThOS, ThOSe and ThOTe under hydrostatic compressive strain.

Compound	Γ	X	X	Z	$\nu_0; \nu_1 \nu_2$
					ν_3
ThOS(-10%)	1	-1	1	-1	(1;1 0 0)
ThOSe(-10%)	1	1	-1	1	(1;0 0 0)
ThOTe(-5%)	1	1	-1	1	(1;0 1 1)

The phonon dispersion profiles of ThOSe and ThOTe are almost similar to that at ambient, but in the case of ThOS, we can see few intermediate frequency optical phonon modes separated out from low frequency phonon modes, which might be due to different atomic masses of elements. Oxygen and sulphur are having comparable atomic masses, and are lighter compared to selenium and tellurium, which could be a reason for these intermediate optical modes to be separated out. In the strained case also the range of phonon frequency is found to be reduced from ThOS to ThOTe. Further, we have extended the electronic structure calculations to examine the topological nature under strained state. Both inversion symmetry as well as time reversal symmetry are preserved under strained state too. Here, we have calculated the Z_2 invariant similar to ambient case, and are given in table 6. From the table, it is evident that all the compounds show strong topological nature.

There exists three highly linearized Dirac points in the same energy range, one at high symmetry point A and two around Γ in the BZ which indicate the presence of nodal line in ThOS (supplementary figure 4(a)). In the case of ThOSe, we found same number of Dirac points, two located at point M and A respectively, and the other one is along Z-R (supplementary figure 4(b)), and nodal line is also possible in this case. In the case of ThOTe, there is one Dirac point along Γ -Z (supplementary figure 4(c)). The presence of highly linearized Dirac points and the possible nodal line joining the Dirac points in the same energy range along with calculated Z_2 invariants are the evidences to claim these compounds as topological metals. Overall, we could see that ThOS and ThOSe turned out to be strong topological materials under strain and ThOTe preserves its strong topological nature under strain. Next, we also analysed the strain effects on thermoelectric coefficients of

ThOCh, but we could not see promising results compared to ambient case, so these are not being discussed here.

5. Monolayer study

5.1. Dynamical and electronic properties

Since all the investigated compounds are having layered structure, we have analysed the monolayer ThOCh. The phonon dispersion for monolayer is shown in figure 9. The positive frequency for phonon modes confirms the dynamical stability of monolayer ThOCh. There is no interaction between optical modes and acoustic modes in case of ThOS but in ThOSe and ThOTe, the low frequency optical modes are interacting with acoustic modes. The schematic of the monolayer and the calculated band structure are given in figures 1(b) and 10 respectively. From the electronic structure calculations, it is evident that four bands are crossing the Fermi level, which implies that monolayer ThOCh are metallic, while the bulk ThOCh are semiconductors. To know about the contribution of individual elements to the bands which are crossing the Fermi level, we have calculated total density of states along with projected density of states and found that 'p' orbitals of oxygen and chalcogens are dominating near Fermi level (figure 11). We have compared the density of states of monolayer with that of bulk and found that there is significant variation at Fermi level. All the investigated monolayers are found to have high value of density of states at Fermi level together with the peaks at Fermi level. In monolayer ThOTe, the peak is exactly at Fermi level with density of states around 5.48 states/eV (figure 11(c)). The presence of peak at Fermi level along with high density of states show the possibility of superconducting nature in monolayer ThOCh [58, 59]. As the investigated compounds are reported as topological materials in bulk form, we have checked the possibility in monolayer too, but the electronic structure calculations of monolayer lacks inversion symmetry and we cannot explore topological nature by calculating Z_2 parameter along TRIM points as done in bulk. From the calculated band structure without spin-orbit coupling in ThOS, three Dirac points can be seen, one along Γ -X and other two lying along M- Γ (figure 10(a)). Similarly, three Dirac points can be seen in case of ThOSe (figure 10(b)). The highly linearized Dirac points in the same

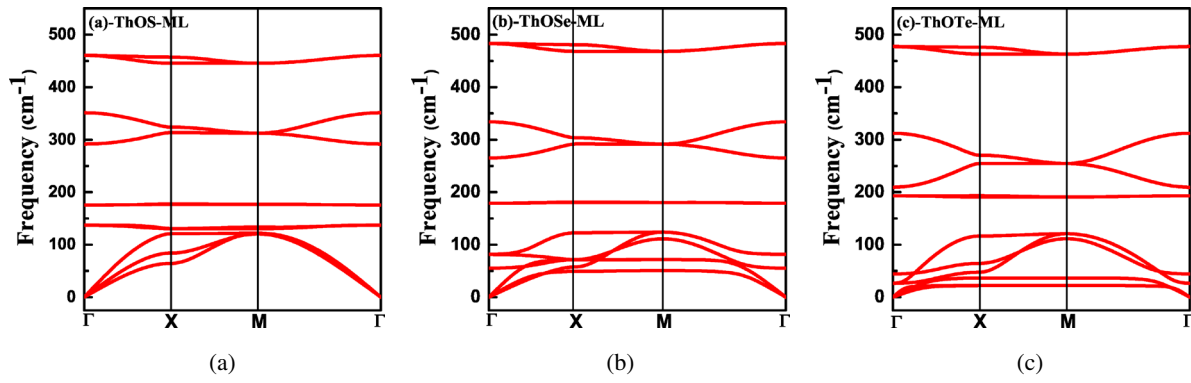


Figure 9. Calculated phonon dispersion for monolayer ThOS (a), ThOSe (b) and ThOTe (c).

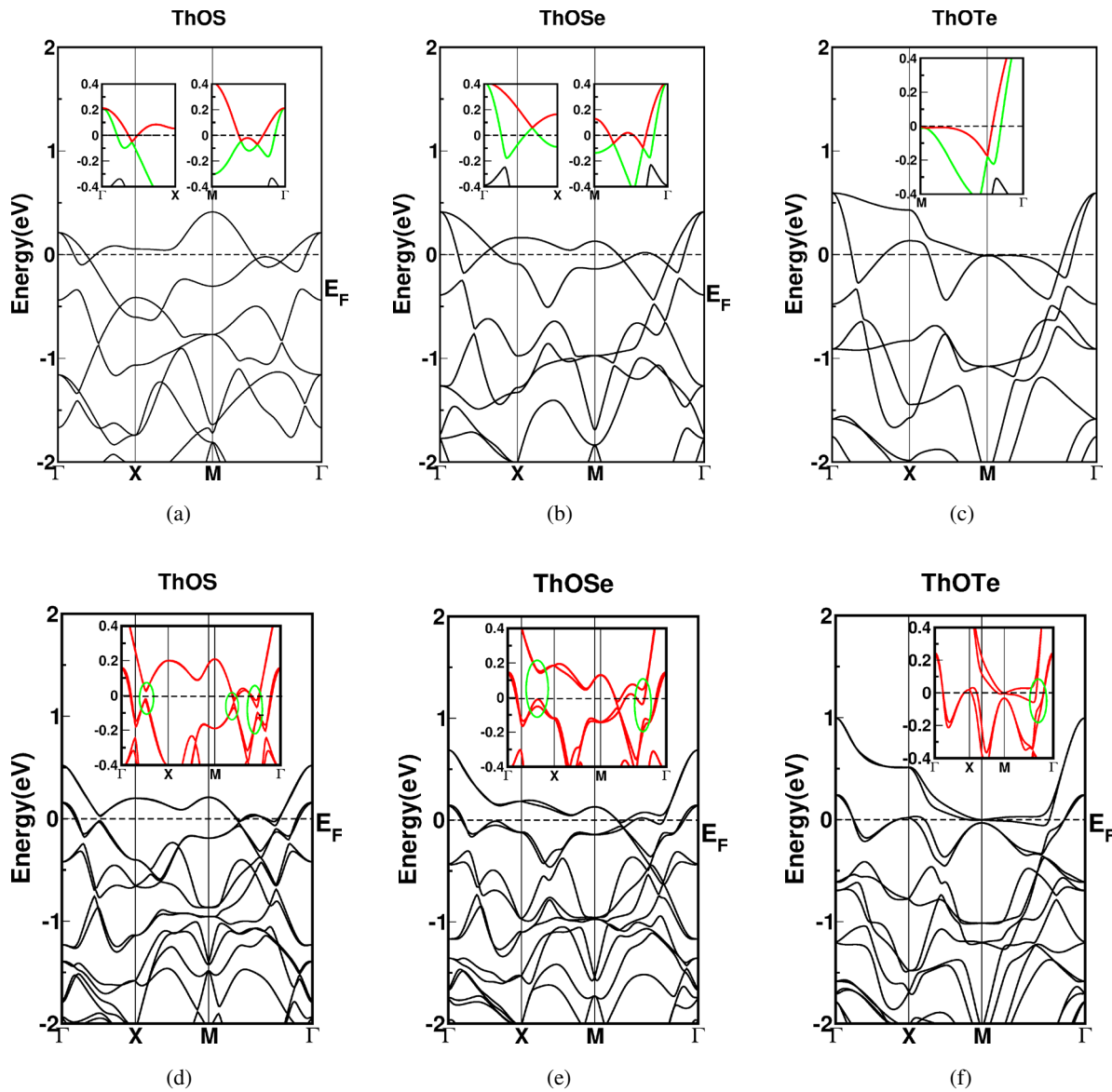


Figure 10. Band structure calculated without spin-orbit coupling in (a), (b) and (c), and with spin-orbit coupling in (d), (e) and (f) in monolayer.

energy range at different high symmetry points in the BZ indicate the presence of nodal line in ThOS and ThOSe without spin-orbit coupling. In this case also, the spin-orbit coupling shows importance like that of bulk and with the inclusion of

the same, these Dirac points are deformed slightly (figures 10(d)–(f)). This variation in band profiles with and without spin-orbit coupling might indicate the topological nature. The edge states band structure calculations are also supporting the

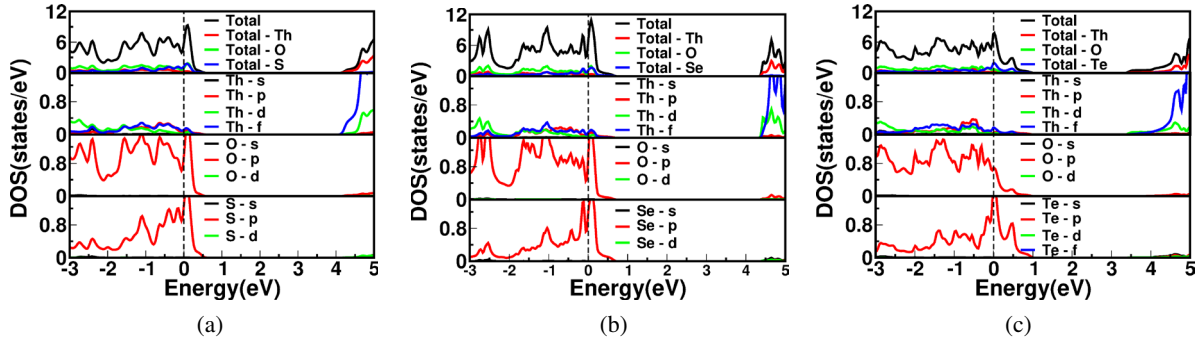


Figure 11. Density of states calculated for ThOS (a), ThOSe (b) and ThOTe (c) in monolayer.

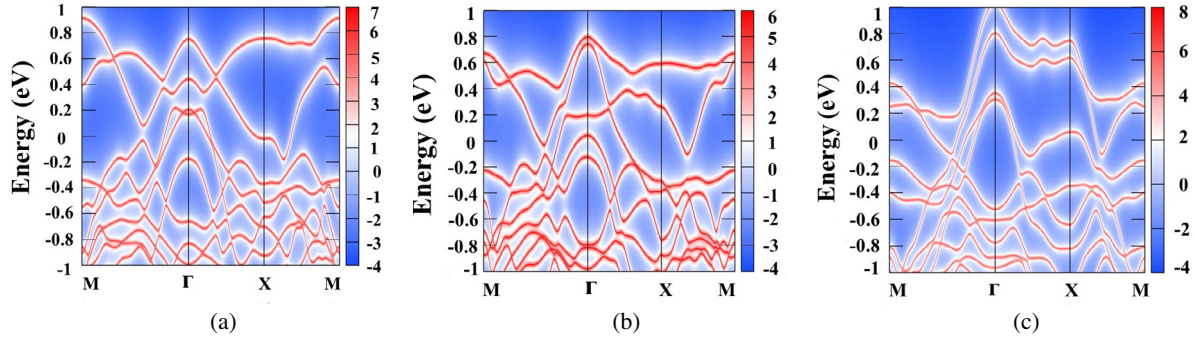


Figure 12. Surface bands calculated for monolayer ThOS (a), ThOSe (b) and ThOTe (c).

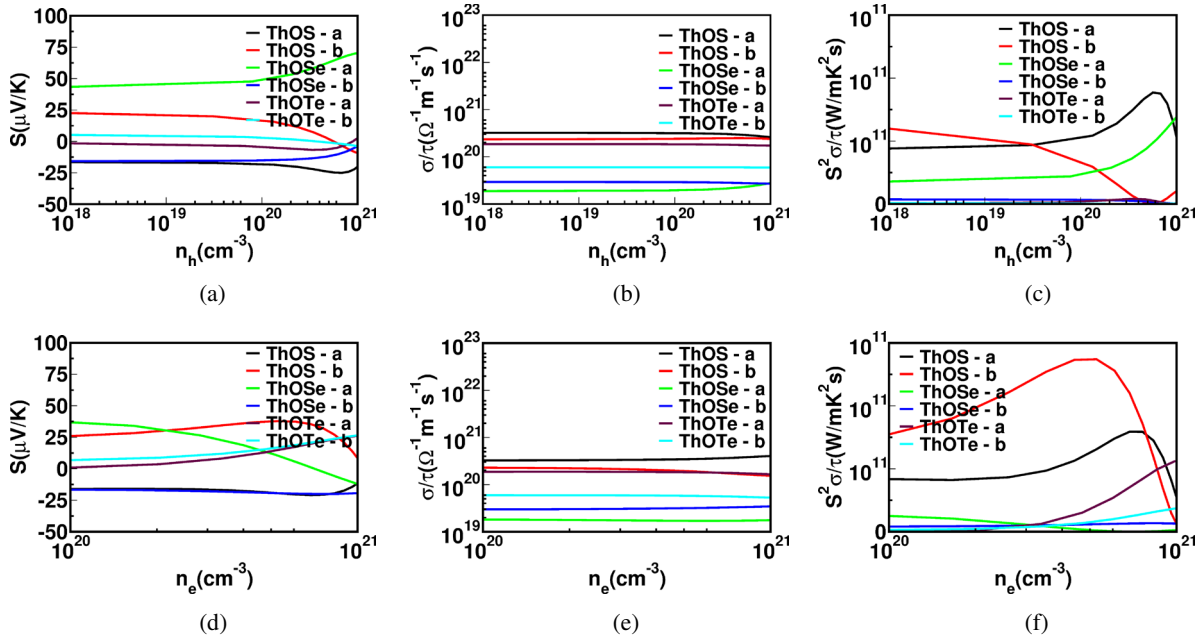


Figure 13. Thermoelectric properties for monolayer calculated as a function of carrier concentration, Thermopower (a) and (d), electrical conductivity scaled by relaxation time (b) and (e), power factor scaled by relaxation time (c) and (f).

same as shown in figure 12. The surface states band structure calculations of ThOS show camels back type of flipping around Γ point, which is an evidence for strong topological metal.

From the calculated electronic properties, the monolayer ThOCh are found to be metallic. To understand the behavior of the bands which are crossing the Fermi level, we have calculated Fermi surfaces. The bands, which are crossing the Fermi level show mixture of hole and electron nature. This

can be understood from detailed discussions, as given below. The Fermi surface of ThOS is cylindrical shaped, centered at Γ point for two bands out of four (supplementary figures 3(a), (b)). This is due to parabolic nature of bands across Fermi level. The Fermi surface for other two bands look like vertical sheets with different faces on both sides directed towards Γ -M for ThOS (supplementary figures 3(c), (d)). This might be due to the mixture of linear and parabolic bands. For ThOSe, the Fermi surface for first two bands are similar to ThOS. The

Fermi surfaces for other two bands are cylindrical in shape directed towards vertices (supplementary figures 3(e)–(h)). In case of ThOTe, the Fermi surface for first two bands are different, a combination of one flattened cylinder around Γ point and thin sheets along Γ -X direction. The cylindrical Fermi surface around Γ point is the signature of two dimensional nature [59]. The present work for monolayer is also reporting the same. The Fermi surface for third band look like more flattened ribbons along Γ -M. This might be due to flattened bands in this direction across Fermi level (supplementary figures 3(i), (j), (k)). In the next section, we would like to discuss the thermoelectric properties of monolayer ThOCh.

5.2. Thermoelectric properties of monolayer

We have calculated thermoelectric properties of monolayer ThOCh along 'a' and 'b' axis where 'a' and 'b' are corresponding to 'x' and 'y' axis respectively. The thermopower calculated for monolayer ThOCh as a function of carrier concentration is shown in figures 13(a) and (d). The thermopower is found to be independent of both carriers for all the compounds. We could see that TE properties of electrons can be calculated for the concentration ranging between 10^{20} – 10^{21} cm^{-3} . Thermopower for holes is found to be carrier independent for a wide range from 10^{18} – 10^{20} cm^{-3} . The magnitude of thermopower is lesser for both the carriers due to metallic character. The electrical conductivity scaled by relaxation time calculated as a function of carrier concentration are given in figures 13(b) and (e). The electrical conductivity scaled by relaxation time is constant for wide range of hole concentration along both 'a' and 'b' axis. The magnitude of electrical conductivity scaled by relaxation time lies between 10^{20} – 10^{21} $\Omega^{-1} \text{m}^{-1} \text{s}^{-1}$ for all the compounds and the corresponding power factor scaled by relaxation time is shown in figures 13(c) and (f). The discussed thermoelectric properties of these layered structures are found to be independent of carriers, which is reflected in power factor scaled by relaxation time also. The magnitude of power factor scaled by relaxation time is almost constant with value around 10^{11} $\text{W mK}^{-2}\text{s}$ for hole concentration ranging between 10^{18} – 10^{20} cm^{-3} . Thermoelectric properties at 700 K are given in supplementary figure 2. TE properties are found to increase with temperature. The highlights of our results are, the electrical conductivity scaled by relaxation time being higher and carrier independent and its value being enhanced by an order of 10 compared to that of bulk.

6. Conclusions

We have calculated electronic, topological and transport properties of the investigated compounds in both bulk and monolayer using density functional theory. In addition to that, the effects of strain on these compounds in bulk are also presented. The extended electronic structure calculations reveal the strong topological insulating nature of ThOTe, and weak topological nature of ThOSe in bulk. Calculated Z_2 parameter,

band inversion and surface states support the same. A semiconductor to metallic transition is observed at 10% hydrostatic compressive strain for ThOS and ThOSe, and at 5% for ThOTe. The phonon dispersion calculations and mechanical properties have been studied and all the compounds are found to be both mechanically and dynamically stable at ambient as well as under hydrostatic compressive strained state. From the extended electronic structure calculations under strain, all the compounds are reported as topological metals. Z_2 invariants along with possible nodal line joining different Dirac points lying in same energy range are the evidences for the same. The electronic structure calculations of monolayer for all the compounds reveal these compounds to be metallic, The presence of Dirac points close to Fermi level in ThOS and ThOSe along with change in band topology due to spin–orbit coupling and surface state calculations confirm these compounds to be topological metals. In addition to that, the existence of peak near Fermi level along with high density of states speculate that, these compounds might turn out to be superconductor in monolayer form. The bulk thermoelectric calculations reveal that ThOS and ThOSe possess promising results for both the carriers which are in good accord with well established compounds at 300 K, while ThOTe is not a good candidate. We have calculated thermal conductivity for one of the investigated compounds which is found to have low thermal conductivity. This low value also support good thermoelectric performance. We believe that the other compounds might also show thermal conductivity in similar range for bulk. The electrical conductivity scaled by relaxation time is found to be high and constant for wide range of hole concentration in monolayer ThOCh. The constant value of electrical conductivity scaled by relaxation time and its enhanced value by an order of 10 compared to that of bulk, make these compounds promising candidate for future 2D thermoelectric devices. In summary, the present study reveals that these compounds have potential applications in the area of thermoelectricity and topological materials which can be explored further.

Acknowledgment

The authors VKS, SPC and VK would like to thank IIT Hyderabad for computational facility. VKS and SPC also would like to thank MHRD for fellowship. VKS, SPC and VK would like to thank CDAC for computational facility.

ORCID iDs

V Kanchana  <https://orcid.org/0000-0003-1575-9936>

References

- [1] Myung-Chul J, Kwan-Woo L and Pickett Warren E 2018 *Phys. Rev. B* **97** 121104
- [2] Mishra S K, Satpathy S and Jepsen O 1997 *J. Phys.: Condens. Matter* **9** 461–70

- [3] Young Steve M, Sugata C, Walter Eric J, Mele Eugene J, Kane Charles L and Rappe Andrew M 2011 *Phys. Rev. B* **84** 085106
- [4] Yonghong Z, Yibin H, Lei L, Yu Z and Hong G 2011 *Nano Lett.* **11** 2088–91
- [5] Zhong W, Xiao-Liang Q and Shou-Cheng Z 2010 *Phys. Rev. Lett.* **105** 256803
- [6] Hasan M Z and Kane C L 2010 *Rev. Mod. Phys.* **82** 4570
- [7] Qi X L and Zhang S C 2011 *Rev. Mod. Phys.* **83** 1057
- [8] Kane C L and Mele E J 2005 *Phys. Rev. Lett.* **95** 146802
- [9] Bernevig B A, Hughes T L and Zhang S C 2006 *Science* **314** 1757
- [10] Ning X, Yong X and Jia Z 2017 *NPJ Quantum Mater.* **2** 51
- [11] Han C Q et al 2015 *Appl. Phys. Lett.* **107** 171602
- [12] Wenshuai G et al 2017 *Phys. Rev. Lett.* **118** 256601
- [13] Binghai Y and Shou-Cheng Z 2012 *Rep. Prog. Phys.* **75** 096501
- [14] Muechler L, Alexandradinata A, Neupert T and Car R 2016 *Phys. Rev. X* **6** 041069
- [15] Topsakal M, Cahangirov S and Ciraci S 2010 *Appl. Phys. Lett.* **96** 091912
- [16] Guinea F, Katsnelson M I and Geim A K 2010 *Nat. Phys.* **6** 30–3
- [17] Brixner L H J 1962 *Inorg. Nucl. Chem.* **24** 257–63
- [18] Revolinsky E and Beersten E 1964 *J. Appl. Phys.* **35** 2086
- [19] Zhiyong Z, Yingchun C and Udo S 2013 *Phys. Rev. Lett.* **110** 077202
- [20] Muhammad S, Ur Rahman A, Ul Haq B, Azmat I, Afaq A and Iftikhar A 2017 *Comput. Condens. Matter* **13** 111–9
- [21] Gerward L, Olsen J S, Benedict U, Luo H, Itie J P and Voigt O 1988 *High Temp. High Press.* **20** 570
- [22] Kanchana V, Vaitheeswaran G, Svane A, Heathman S, Gerward L and Olsen J S 2014 *Acta Cryst. B* **70** 709468
- [23] Amari S, Mabih S, Abbar B and Bouhafis B 2014 *J. Nucl. Mater.* **704** 186
- [24] Anayas M, Jha P K and Sanyal S P 2005 *Indian J. Pure Appl. Phys.* **43** 109
- [25] Yong X, Zhongxue G and Shou-Cheng Z 2014 *Phys. Rev. Lett.* **112** 226801
- [26] Chen C et al 2017 *Phys. Rev. B* **95** 125126
- [27] Mofazzel M et al 2017 *Phys. Rev. B* **95** 161101
- [28] Koscielski Lukasz A, Emile R, Van Duyne R P, Ellis Donald E and Ibers James A 2012 *Inorg. Chem.* **51** 8112–8
- [29] Hsieh Timothy H et al 2012 *Nat. Commun.* **3** 982
- [30] Pouyan G, Mong Roger S K and Moore J E 2010 *Phys. Rev. Lett.* **105** 166603
- [31] Li-Dong Z et al 2014 *Nature* **508** 373
- [32] Kresse G and Furthmüller J 1996 *Comput. Mat. Sci.* **6** 15
- [33] Kresse G and Furthmüller J 1996 *Phys. Rev. B* **54** 11169
- [34] Atsushi T and Isao T 2015 *Scr. Mater.* **108** 1–5
- [35] Xavier G and Changyol L 1997 *Phys. Rev. B* **55** 10355
- [36] Blaha P, Scwarz K, Sorantin P and Tricky S B 1990 *Comput. Phys. Commun.* **59** 399–415
- [37] Perdew J P, Burke K and Ernzerhof M 1996 *Phys. Rev. Lett.* **77** 3870
- [38] Monkhorst H J and Pack J D 1976 *Phys. Rev. B* **13** 5188
- [39] Marzari N, Mostofi A A, Yates J R, Souza I and Vanderbilt D 2012 *Rev. Mod. Phys.* **84** 1419
- [40] QuanSheng W, ShengNan Z, Hai-Feng S, Matthias T and Soluyanov Alexey A 2018 *Comput. Phys. Commun.* **224** 405–16
- [41] Sancho M L, Sancho J L and Rubio J 1985 *J. Phys. F: Met. Phys.* **15** 851
- [42] Madsen G K H and Singh D J 2006 *Comput. Phys. Commun.* **175** 67
- [43] Scheidemantel T J, Ambrosch-Draxl C, Thonhauser T, Badding J V and Sofo J O 2003 *Phys. Rev. B* **68** 125210
- [44] Jodin L, Tobola J, Pecheur P, Scherrer H and Kaprzyk S 2004 *Phys. Rev. B* **70** 184207
- [45] Chaput L, Pecheur P, Tobola J and Scherrer H 2005 *Phys. Rev. B* **72** 085126
- [46] Atsushi T, Laurent C and Isao T 2015 *Phys. Rev. B* **91** 094306
- [47] Liang F, Kane C L and Mele E J 2007 *Phys. Rev. Lett.* **98** 106803
- [48] Born M and Huang K 1956 *Dynamical Theory of Crystal Lattices* (Oxford: Clarendon)
- [49] Hill R 1952 *Proc. Phys. Soc. Lond. A* **65** 349
- [50] David B, Jing L, Emile A, Sunanda M, Jiche S, Wei C and Nita D 2015 *Materials* **8** 1043–58
- [51] Ding J et al 2015 *New J. Phys.* **17** 083012
- [52] Clarke D R 2003 *Surf. Coat. Technol.* **163** 67
- [53] Clarke D R and Levi C G 2003 *Annu. Rev. Mater. Res.* **33** 383
- [54] Chandran Anoop K, Vijay Kumar G, Sreeparvathy P C and Kanchana V 2016 *J. Solid State Chem.* **243** 198–206
- [55] Guo L B, Wang Y X, Yan Y L, Yang G, Yang J M and Feng Z Z 2014 *J. Appl. Phys.* **116** 033705
- [56] San-Dong G 2016 *RSC Adv.* **6** 47953
- [57] San-Dong G 2018 *Phys. Chem. Chem. Phys.* **20** 7236
- [58] Singh David J 2012 *New J. Phys.* **14** 123003
- [59] Lebegue S 2007 *Phys. Rev. B* **75** 035110